Available online at www.sciencedirect.com
SCIENCE DIRECT®
International Journal of Multiphase Flow 31 (2005) 940–956
International Journal of Multiphase Flow
www.elsevier.com/locate/ijmulflow

Effect of near-wall turbulence enhancement on the mechanisms of particle deposition

Lorenzo Botto [a,b,1], Chidambaram Narayanan [a], Marco Fulgosi [a], Djamel Lakehal [a,*]

[a] *Institute of Energy Technology, Swiss Federal Institute of Technology, ETH-Zentrum/CLT, CH-8092 Zurich, Switzerland*
[b] *Department of Energy Technology, University of Udine, Italy*

Received 9 July 2004; received in revised form 11 May 2005

Abstract

The modification of deposition mechanisms of small particles in wall turbulence due to enhanced near-wall fluctuations is presented. The direct numerical simulation database of turbulent air flow over a water surface populated by gravity-capillary waves of small wave slope was used to mimic the enhancement in fluctuation intensity. Lagrangian tracking of particles is performed under the assumption of one-way coupling between the particles and the flow. Two sets of particles have been considered with inertial response times of 5 and 15, respectively, normalized using the friction velocity at the air–water interface and the kinematic viscosity of air. Compared to wall-bounded flow, the particle deposition rates on the interface were found to be considerably higher; specifically for the low-inertia particles, an eightfold increase was observed. The deposition rate for particles of higher inertia increased by only 60%. The correlation characterizing particle deposition rates for wall-bounded flows, where the deposition rate is proportional to the square of the particle response time, was found to be invalid for the flow with enhanced near-wall turbulence. Comparison with experimental results on particle deposition onto rough walls showed better correlation. Depositing particles were divided into *free-flight* and *diffusional deposition* populations. Since the primary effect of the interfacial waves is to increase the turbulence intensity in the near-interface region with high particle concentration, a remarkable increase in diffusional deposition is observed. As in wall-

* Corresponding author. Tel.: +41 1 632 4613; fax: +41 1 632 1166.
E-mail address: lakehal@iet.mavt.ethz.ch (D. Lakehal).
[1] Present address: Johns Hopkins University, United States.

0301-9322/$ - see front matter
doi:10.1016/j.ijmultiphaseflow.2005.05.003

bounded flows, diffusional deposition is seen to be the dominant mechanism of deposition. The free-flight mechanism, where particles acquire velocities high enough to travel directly to the interface, remains unaffected by enhanced near-wall velocity fluctuations.

Keywords: Particle tracking; Deposition; Turbulence

1. Introduction

A recent study by the present authors (Narayanan et al., 2003) has shown that due to the strong accumulation of particles very near the wall, particle deposition induced by residual turbulent fluctuations in the near-wall region (*diffusional deposition*) could dominate over the so-called *free-flight* mechanism of particle deposition. It could then be conjectured that even a small increase in turbulence intensity in this region could result in a large increase in deposition rates. For example, in the case of rough walls, experiments (Chamberlain, 1967; El-Shobokshy, 1983) have shown that the deposition rate of particles is enhanced when the surface roughness increases. Verification of the above conjecture and understanding the modifications to particle deposition mechanisms, are the primary motivations behind this study.

With this goal in mind, the counter-current air–water flow direct numerical simulation (DNS) database of Fulgosi et al. (2003) was employed to mimic the effect of enhanced near-wall turbulence (similar to roughness elements). The small amplitude gravity-capillary waves created by the interplay between shear, surface tension, and gravity on the water surface have the effect of enhancing near-interface velocity fluctuations. Evidently, other methods of reproducing the effect of roughness elements could be used (Miyake et al., 2002), however, the in-house spectral database of Fulgosi et al. (2003) was chosen for reasons of reliability and convenience. The methodology in Narayanan et al. (2003) is used to analyze the effect of the interfacial motion on turbulent deposition. The effect of gravity is neglected in the particle equation of motion with the intention of comparing the deposition statistics to a vertical channel/pipe flow, where gravity might not strongly influence deposition. The influence of gravity in particle deposition has been studied by Zhang and Ahmadi (2000) and in a recent work by Mito and Hanratty (2003). It was shown (Zhang and Ahmadi, 2000) that particle deposition is enhanced when gravity is in the direction of the flow, and is reduced when gravity is opposing the flow direction, particularly when the shear velocity is low. This effect is caused by the shear induced lift force, which becomes significant. For horizontal channels, the effect of gravity on deposition is direct and deposition increases due to gravitational sedimentation.

The study of particle deposition has attracted significant attention in the past decades because of its relevance to numerous industrial applications. Friedlander and Johnstone (1957) pioneered the research on particle deposition by proposing the so-called free-flight deposition theory. In this model, particles are transported by turbulent motion to within one *stop-distance* of the wall, where they acquire sufficient inertia to coast through the viscous sub-layer and to deposit. Subsequently, the free-flight concept has been the starting point of many theories of particle deposition (Cleaver and Yates, 1975; El-Shobokshy and Ismail, 1980).

Direct numerical simulation of a turbulent channel flow with particles (McLaughlin, 1989) showed that particles gradually accumulated in the viscous sub-layer and had large residence

times in this region. The duration of the simulation was, however, too short to obtain steady-state deposition rates, because the accumulation process continued to occur even until the end of the simulation period. Rashidi et al. (1990), describing an experiment in which particles were released in an open-channel flow, emphasized the importance of sweep ejection events in depositing and re-entraining particles. They reported an accumulation of particles near the wall and observed that particles with radii less than 0.5 wall units, approaching very close to the wall, are rarely lifted up by wall ejections. The above observations have been confirmed by Kaftori et al. (1995), where the motion of particles was found to be intimately related to the action of quasi-streamwise vortices populating the near-wall region. From a statistical point of view, the migration of particles from the bulk towards the wall has been attributed to *turbophoresis*, which causes a net particle flux from regions of higher turbulence intensity to regions of lower turbulence intensity (Reeks, 1983). In a recent DNS study, Marchioli and Soldati (2002) presented a mechanistic explanation for the accumulation of particles in the near-wall region, based on the sweep-ejection cycle and turbulence regeneration mechanisms.

Brooke et al. (1992) employed DNS to study particle deposition in a turbulent channel to evaluate the free-flight theory. Looking at the probability density function (PDF) of the vertical near-wall particle velocities, they found that only a small fraction of particles have a velocity high enough to execute a free-flight to the wall. This fact is at odds with the original free-flight model, where all depositing particles are supposed to move on a free-flight path to the wall. In a subsequent paper, Brooke et al. (1994) reported that deposition was dominated by particles executing free flights to the wall. However, noting the process of particle accumulation near the wall, they mention the possibility of particle deposition due to random fluid velocity fluctuations in this region (referred to as diffusional deposition), even though in their simulations such a deposition flux was insignificant.

An important point with regard to the above studies (McLaughlin, 1989; Brooke et al., 1992, 1994) is that in their simulations the mean particle concentration remained in a state of evolution due to the short simulation times. The velocities of the depositing particles were found to be high, implying that deposition was predominantly caused by free-flight. However, since a large fraction of the total particle flux towards the wall does not have a velocity high enough to deposit by free-flight, continued particle accumulation near the wall could be expected. In order to reach a steady-state, additional mechanisms of deposition have to gain in importance to balance the wallward flux. By carrying out simulations up to a statistically steady-state, Narayanan et al. (2003) have shown that, contrary to the prevalent notion, it is the near-wall diffusional deposition that is the dominant mechanism of deposition.

Narayanan et al. (2003) used the methodology presented by van Haarlem et al. (1998), which differed from previous numerical work in that it allowed the particle field to reach a statistically stationary state through the reintroduction of deposited particles into the flow. Narayanan et al. (2003) divided the depositing particles into two distinct populations: those having large deposition velocities and small near-wall residence times, and those having negligible wall-normal velocities and large near-wall residence times. The first class was referred to as the *free-flight* population and the second as the diffusional deposition population. Diffusional deposition was found to be the dominant mechanism of deposition for the particle response times studied. The free-flight mechanism was shown to account for 40% of the deposition for the heavier particles considered.

The objective of the present study is to address the modification of particle deposition mechanisms due to increased near-wall fluctuation intensity, as compared to the widely documented case of particle transport in smooth wall bounded flows. The outline of the presentation is as follows: The transport equations and the simulation procedure adopted for the continuous phases and the particles are presented in Section 2. Results of the simulations are discussed in separate sections dealing with the characteristics of the interfacial waves, particle dispersion, and deposition mechanisms. The results are then summarized along with important conclusions.

2. Governing equations and numerical method

2.1. Continuous phases

The spectral DNS database of stratified air–water flow configuration (Fig. 1) presented by Fulgosi et al. (2003) was used to mimic enhanced near-wall fluctuation intensity and its influence on particle deposition. The air and water streams flow in opposite directions and the interface is free to deform under the effect of the shear imposed by the relative motion. This destabilizing force is balanced by gravity and surface tension. The two fluids are considered to be incompressible, isothermal, and Newtonian. The reference quantities used for normalization in each continuous phase $k = \mathrm{a}, \mathrm{w}$ (denoting air and water), are the effective shear velocity $u_{\bigstar k}$, half the height of each computational domain $h_\mathrm{a} = h_\mathrm{w} = h$, and the kinematic viscosity ν_k. When the interface is flat, at the beginning of the simulation, the interfacial shear exactly balances the imposed mean pressure gradient, so that $u_\bigstar$ corresponds to the shear velocity $u_\tau = \sqrt{\tau_\mathrm{int}/\rho_k}$ in wall-bounded flows. As the interfacial waves start to develop, part of the energy goes into overcoming the form drag and the interfacial shear reduces, leading to $u_\tau = 0.986 u_\bigstar$ in this case (Fulgosi et al., 2003).

The shear-based Reynolds number, defined using the initial shear velocity is $Re_\bigstar = u_\bigstar 2h/\nu = 171$ in each phase. The nondimensional time is defined by $t^+ = t u_\bigstar^2/\nu$ in wall units. The nondimensional lengths in wall units have been normalized by $\nu/u_\bigstar$. Considering the situation where

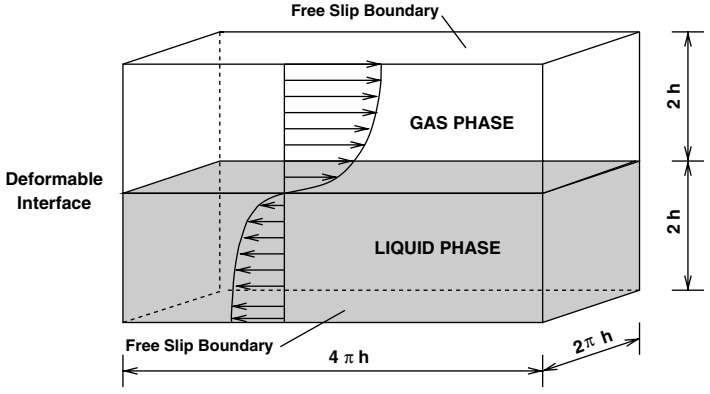

Fig. 1. Geometry of the simulated air–water stratified flow.

the dispersed phase does not influence the continuous phase (one-way coupling), the governing equations for each of the continuous phases can be written in nondimensional form as

$$\nabla \cdot \mathbf{u}^+ = 0, \tag{1}$$

$$\frac{\partial \mathbf{u}^+}{\partial t^+} + \mathbf{u}^+ \nabla \cdot \mathbf{u}^+ = -\nabla p^+ + \frac{1}{Re_\star} \nabla^2 \mathbf{u}^+, \tag{2}$$

where $\mathbf{u}^+$ is the fluid velocity vector normalized by $u_\star$, and p^+ is the dynamic pressure normalized by $\rho u_\star^2$.

At the interface, the air and water flows are coupled by enforcing continuity of velocities and stresses. These interfacial continuity conditions can be expressed in nondimensional form as

$$\begin{cases} \frac{1}{Re_\star}((\sigma_{\mathrm{w}}^+ - \sigma_{\mathrm{a}}^+) \cdot \mathbf{n}) \cdot \mathbf{n} + p_{\mathrm{a}}^+ - p_{\mathrm{w}}^+ + \frac{1}{We} \nabla \cdot \mathbf{n} - \frac{1}{Fr} f^+ = 0, \\ ((\sigma_{\mathrm{w}}^+ - \sigma_{\mathrm{a}}^+) \cdot \mathbf{n}) \cdot \mathbf{t}_i = 0, \quad i = 1, 2, \\ \mathbf{u}_{\mathrm{w}}^+ = \mathscr{C} \mathbf{u}_{\mathrm{a}}^+, \end{cases} \tag{3}$$

where σ^+ stands for the viscous stress tensor, f^+ for the vertical displacement of the interface, and $\mathbf{n}$ and $\mathbf{t}_i$ denote the normal and two tangential unit vectors at the interface, respectively. The quantity $\mathscr{C} = \sqrt{\rho_{\mathrm{w}}/\rho_{\mathrm{a}}}$ was taken equal to 29.9, corresponding to air–water flow at atmospheric pressure and 320 K. The Weber (We) and Froude (Fr) numbers are defined using the water shear velocity $u_{\star w}$, as

$$Fr = \frac{u_{\star \mathrm{w}}^2 \rho_{\mathrm{w}}}{gh(\rho_{\mathrm{w}} - \rho_{\mathrm{a}})}; \quad We = \frac{\rho_{\mathrm{w}} h u_{\star \mathrm{w}}^2}{\gamma}, \tag{4}$$

where γ stands for the surface tension coefficient.

The interface motion was computed by solving an advection equation for the vertical elevation of the interface given by $\partial f^+/\partial t + \mathbf{u}^+ \cdot \nabla f^+ = 0$. Since this numerical method cannot handle strong deformations of the interface such as wave breaking, We and Fr, which stabilize the interface deformation, were appropriately chosen. On the basis of scaling arguments they were set equal to 4.8×10^{-3} and 8.7×10^{-5}, respectively, to limit the wave slope. Free slip conditions were employed at the outer boundaries, and periodic boundary conditions were applied in the streamwise and spanwise directions.

At each time step the distorted physical domain is mapped onto a rectangular parallelepiped (DeAngelis et al., 1997), on which the velocity and pressure fields are solved using a Fourier–Chebychev, pseudo-spectral collocation method. For complete details, the reader is referred to Fulgosi et al. (2003). The dimensions of the computational domain for each of the continuous phases are $4\pi h \times 2\pi h \times 2h$, which corresponds to $l_x = 1074$, $l_y = 537$, and $l_z = 171$ wall units in the streamwise, spanwise, and vertical directions, respectively. The spatial grid resolution employed in each computational domain is $64 \times 64 \times 65$, which had proven satisfactory. The flow was computed with a constant time step of $\Delta t^+ = 0.03$ and flow fields were saved every 20 time steps; the resulting time interval of $\Delta t^+ = 0.6$ was found adequate based on a Fourier time series analysis of the flow field. The particles were tracked separately using the stored flow database.

2.2. Dispersed phase

The motion of particles is obtained by solving a set of ordinary differential equations for the individual particle velocity and position. For particles much denser than the fluid ($\rho_p/\rho_a \gg 1$), with diameters smaller than the Kolmogorov length scale, Elghobashi and Truesdell (1992) showed that the only significant forces acting on the particles are the Stokes drag, the buoyancy, and the Basset forces. They also demonstrated that the Basset force was an order of magnitude smaller than drag and buoyancy. Because the present work focuses on deposition and dispersion caused by turbulence and intends to make a comparison with deposition in a vertical channel/pipe flow, the buoyancy force is not taken into account. With the above simplifications, the Lagrangian equation for the particle velocity derived by Maxey and Riley (1983) reduces to

$$\frac{d\mathbf{u}_p}{dt} = -\frac{3}{4}\frac{C_D}{d_p}\left(\frac{\rho_a}{\rho_p}\right)|\mathbf{u}_p - \mathbf{u}|(\mathbf{u}_p - \mathbf{u}), \tag{5}$$

where C_D denotes the drag coefficient given by

$$C_D = \frac{24}{Re_p}(1 + 0.15Re_p^{0.687}) \tag{6}$$

in which Re_p is the particle Reynolds number ($Re_p = d_p|\mathbf{u}_p - \mathbf{u}|/\nu_a$). The empirical correlation for C_D (Clift et al., 1978) is necessary because Re_p does not remain small for depositing particles (McLaughlin, 1989). For particles strictly in the Stokes regime ($Re_p \ll 1$), Eq. (5) simplifies to

$$\frac{d\mathbf{u}_p}{dt} = -\frac{(\mathbf{u}_p - \mathbf{u})}{\tau_p}, \tag{7}$$

where τ_p ($= \rho_p d_p^2/18\mu_a$) is the particle response time. The instantaneous particle location is then obtained by solving $d\mathbf{x}_p/dt = \mathbf{u}_p$.

Other authors (McLaughlin, 1989; Wang et al., 1997) have also considered the Saffman lift force that could be important near the interface because of the mean shear. McLaughlin (1989) showed that the inclusion of the lift force resulted in a higher deposition rate. However, Wang et al. (1997) found that neglecting the lift force resulted in only a slight reduction in the deposition rate.

A Lagrangian particle tracking code (Narayanan et al., 2002) has been used to track particles in the flow field. The code interpolates fluid velocities at discrete grid nodes onto the particle positions. With this velocity, Eq. (5) is integrated in time. For the simulations presented here, 10^5 particles were tracked using fourth-order Runge–Kutta time integration and fourth-order Lagrangian polynomial interpolation. At the start of the simulation, particles were distributed homogeneously in the air flow domain and their initial velocity was set equal to the fluid velocity. The simulation was run for a period of approximately 2500 nondimensional time units. Two sets of particles with nondimensional response times of $\tau_p^+ = 5$ and 15 were chosen. The corresponding particle diameters in wall units were $d_p^+ = 0.3$ and 0.5, respectively.

2.2.1. Particle-phase boundary conditions

For particles leaving the domain through the outflow plane or in the spanwise direction, periodic boundary conditions were applied for both the position and the velocity of the particle. The interface and the free-slip boundaries were considered to be completely absorbing, so that a particle at a

distance less than one particle radius from these boundaries is assumed to have deposited and is removed. Since the total number of particles has to be maintained constant in time to reach statistically stationary conditions, a particle is reintroduced in the domain at the inflow plane ($x^+ = 0$) whenever a particle deposits at the interface or at the upper free-slip boundary. The reintroduced particles were distributed homogeneously at the inflow plane and their velocity was set equal to the fluid velocity at that position. This procedure introduces a constraint on the velocity of the reintroduced particles which is necessarily affected by the imposed initial conditions for a certain time duration.

According to van Haarlem et al. (1998), the distance covered by a $\tau_p^+ = 15$ particle before its velocity becomes independent of the initial conditions is approximately ten times the height of the channel (1710 wall units in the present work). As this length is of the order of the streamwise extent of the fluid domain, a longer domain was adopted for tracking the particles. The streamwise extent of this domain was set to $5 \times l_x$, whereas the spanwise and vertical dimensions were those used for computing the fluid phase. The dimensions of the computational domain in which the particles were tracked were thus, $L_x = 5370$, $L_y = 537$ and $L_z = 171$ wall units in the streamwise, spanwise, and vertical directions, respectively. The fluid velocity in the extended domains was obtained simply by a periodic extension of the flow in the streamwise direction. Only particles located more than 1710 wall units away from the inflow plane were considered for analysis. This method by van Haarlem et al. (1998) offers a twofold advantage: firstly, it allows the particle phase to reach a statistically steady-state due to the reintroduction process, and secondly, particle statistics can be computed as a function of both the vertical and the streamwise directions without any effect of the imposed inflow conditions.

3. Characteristics of the continuous phase

In this section, quantities of importance in explaining the behaviour of the dispersed phase in the flow over the deformable interface (hereinafter referred to as *deformable boundary*, DB) are compared to wall-bounded flow data (hereinafter referred to as *rigid boundary*, RB) at the same shear-based Reynolds number.

The topology of the waves developing over a deformable, sheared air–water interface depends on the intensity of the interfacial shear stress. The time spectrum of the nondimensional wave elevation (at the center of the interface) is shown in Fig. 2. The spectrum was obtained over a time interval of 350 large-scale (h/U_0, where U_0 is the mean streamwise velocity) time units. The most energetic wave period was found to be $T_{ls} = 20$ large-scale time units, in agreement with measurements (McCready and Hanratty, 1985). The maximum waveslope never exceeded $ak \approx 0.01$ (where a is the amplitude and k is the wavenumber) and the root mean square (rms) wave displacement in wall units was found to be $f_{rms}^+ \approx 0.7$.

In their detailed investigation of the turbulent fields in the DB and RB cases, Fulgosi et al. (2003) observed similar distributions for the first (mean) and second (rms) moments of the PDF of the velocity fluctuations. The main differences, as expected, were located near the interface, where the difference in boundary conditions led to non-zero values for the turbulence intensities in the DB case (see Fig. 4) and in some higher order statistics. These results are not presented here to avoid repetition.

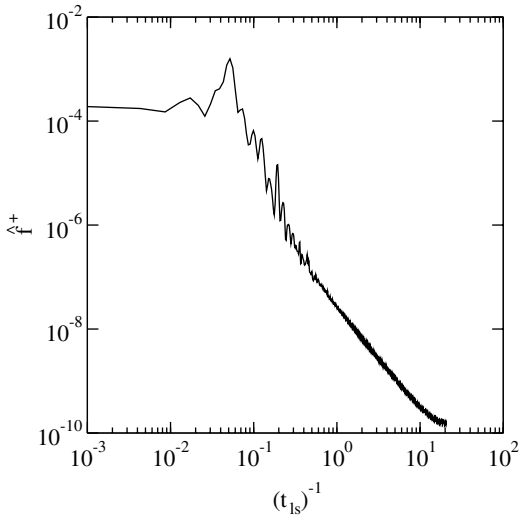

Fig. 2. Time spectrum of the interface motion.

4. Characteristics of the particle phase

Two different sets of particles with nondimensional response times of 5 and 15 have been considered in this investigation. For both particle response times, a large increase in the deposition rate has been found for the DB case. In the following sections the reasons for such an increase will be examined, starting with particle phase mean and rms velocities, concentration profiles, and statistics describing deposition mechanisms. At every stage, a one-to-one comparison with the results obtained by Narayanan et al. (2003) for the RB case will be presented.

4.1. Particle velocity statistics

Fig. 3(a) presents the particle-phase mean vertical velocity. Even though the fluid has a zero mean vertical velocity, the particles have a nonzero mean vertical velocity. This is consistent with the fact that for deposition to occur, particles must have a mean drift velocity towards the boundaries. The mean vertical velocity is the same for both flow configurations. The velocity towards the lower boundary is higher for $\tau_p^+ = 15$ particles, meaning that turbophoresis is more efficient in transporting these heavier particles towards the interface/wall. Qualitatively similar results have been presented for a pipe flow problem (Young and Leeming, 1997).

The particle mean vertical velocity is a result of the interaction of particles with the fluid turbulence. This velocity is created and maintained by a balance between two turbulence diffusion effects, namely turbophoresis, resulting in a systematic average motion of particles from regions of higher to lower turbulence intensity, and turbulent mixing of the concentration gradients existing in the vertical direction (see Fig. 5(b)). Briefly, it has been shown that, turbophoretic transport from the bulk towards the wall is the same in both the flows.

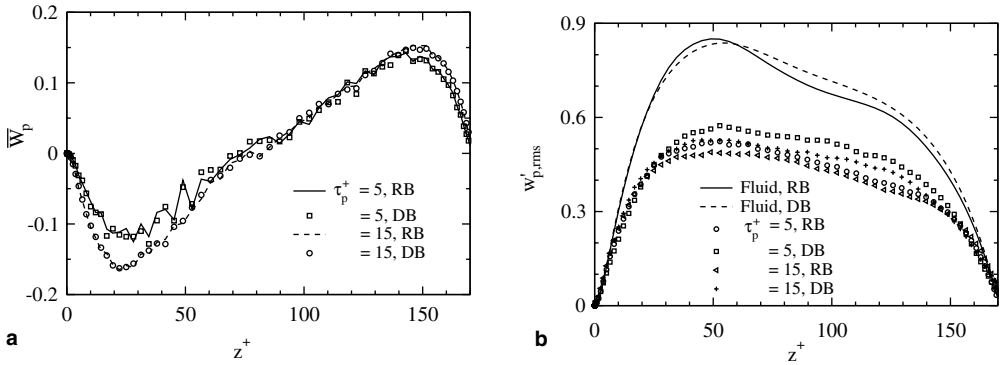

Fig. 3. (a) Mean particle vertical velocity and (b) rms of particle vertical velocity.

4.2. Particle turbulence intensity

Fig. 3(b) shows the rms vertical velocity fluctuations for the fluid phase in both flows and for the particles. The turbulence intensity for the higher inertia particles is lower in the bulk flow. The fluctuation intensity for both particle inertias is seen to be marginally higher in the DB case; not much different from the small differences between the two flows.

4.2.1. Near-interface turbulence intensity

The near-interface region is of critical importance in this study, since the modification of the deposition mechanisms by the increased velocity fluctuations is of primary interest. A small change in the turbulence properties in this region can produce a significant change in the deposition rate, because of the high concentration of particles in the near-interface region. The near-interface normal velocity fluctuation is presented in Fig. 4. The rms of particle vertical velocity fluctuations remains nonzero approaching the interface, with the heavier particles having a higher value in both flows. For the DB case, the fluid fluctuation intensity itself remains nonzero at the

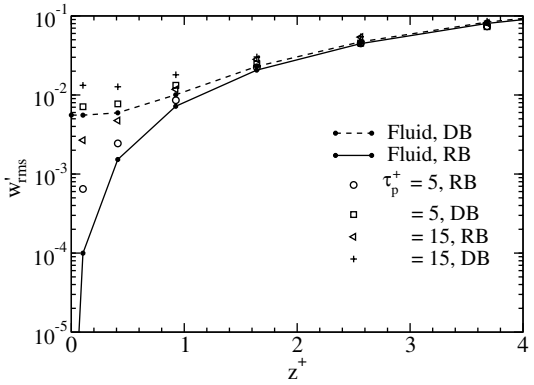

Fig. 4. RMS of vertical velocity for the continuous and dispersed phases in the region adjacent to the interface/wall.

interface due to the interfacial motion; the particles, therefore, have an even higher intensity of fluctuations in this region.

Higher turbulence intensity for the particles in the near-wall and interfacial regions as compared to the fluid can be attributed to the inertial overshoot phenomenon (Narayanan et al., 2003) where, due to their inertia, particles overshoot the local fluid turbulence intensity as they arrive from regions of higher turbulence intensities. This notion will be reinforced in the next section on deposition mechanisms, where attention will be paid to the free-flight particles that deposit with velocities much larger than the ambient fluid velocity. The free-flight particles are examples of the overshoot phenomenon.

4.3. Concentration profiles

Variation of the average particle concentration along the vertical direction, $\langle C\rangle_y^t$, is shown in Fig. 5. Time averaging was performed after a statistically stationary state was reached (see Fig. 6). The distribution shown refers to a region located in the center of the computational domain ($x^+ = 2400-2600$) with a constant vertical bin height of $\Delta z^+ = 0.15$. The time- averaged concentration in every slab was normalized by the average concentration of particles in the region considered (i.e. setting the average equal to unity). A large increase in particle concentration very close to the lower boundary is observed in all cases. Such an accumulation near the wall has also been observed in other studies (McLaughlin, 1989; Rashidi et al., 1990; van Haarlem et al., 1998; Marchioli and Soldati, 2002) in both numerical simulations and experiments.

Peak values of concentration occur at $z^+ \approx 1$ for the DB case for both particle inertias. In the RB case, the peak in the concentration is at $z^+ \approx 0.4$, which is close to the nondimensional particle diameters. The main difference between the two flows is the much lower accumulation in the DB case, which can be directly attributed to the higher deposition rates. The drift velocity of particles moving towards the lower boundary due to turbophoresis is the same for both flows for a given particle response time (see Fig. 3(b)). Therefore, it is natural to expect higher equilibrium concentration for the RB case given the lower deposition rates. A higher accumulation very close to the lower boundary reduces the concentration of particles in the bulk, thus reducing the particle number/mass flux towards the boundary, which, at equilibrium, is balanced by the deposition flux. In

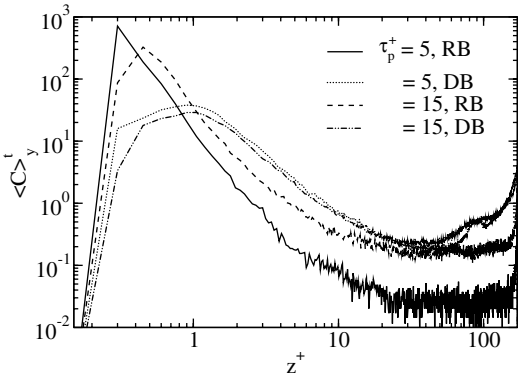

Fig. 5. Mean concentration profiles in the center of the computational domain ($x^+ = 2400$–2600).

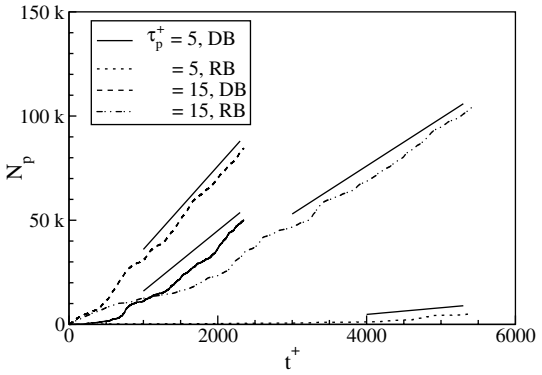

Fig. 6. Cumulative number of droplets deposited with time.

other words, particle concentration near the interface will increase until the deposition flux balances the flux of particles towards the interface due to turbophoresis.

4.4. Deposition rate

The cumulative number of particles depositing as a function of time for the RB and DB cases is shown in Fig. 6. An examination of the trend of deposition reveals that the slopes of the curves reach an asymptotic value after approximately $t^+ > 1000$ (except for the $\tau_p^+ = 5$ particles in the RB case where a longer time is required). Linear fits to the curves are shown in the figure to indicate an approximate constant slope interval which was used for averaging. This suggests that an average rate of deposition can be estimated for the particles depositing at the interface and at the wall. The deposition rate is found to be a strong function of particle inertia, being larger for $\tau_p^+ = 15$ than for $\tau_p^+ = 5$.

The nondimensional deposition coefficient (van Haarlem et al., 1998) is defined as

$$K_d^+ = \frac{J_w}{C_m u_\star}, \tag{8}$$

where J_w is the mass flux of particles reaching the surface considered, C_m is the mean bulk concentration of particles, and $u_\star$ is the friction velocity. The coefficient, calculated at several streamwise positions by dividing the computational domain into slabs of $\Delta x^+ = 200$ wall units and time averaging is shown in Fig. 7(a). The undulations in the deposition coefficient correspond to the periodic extension of the flow domain. Note that the deposition coefficient for $\tau_p^+ = 5$ particles has increased dramatically due to the waves, becoming almost equal to the deposition rate for $\tau_p^+ = 15$ particles.

The deposition coefficients at the deformable interface are compared in Table 1 to those at the solid wall (Narayanan et al., 2003) and to other numerical and experimental data. The values in this table represent average values of the streamwise variation shown in Fig. 7(a). The main observation is the manyfold increase in the deposition rate of $\tau_p^+ = 5$ particles compared to the wall-flow data. The deposition for $\tau_p^+ = 15$ also increases significantly (by 60%), but is moderate compared to the increase for the lower inertia particles.

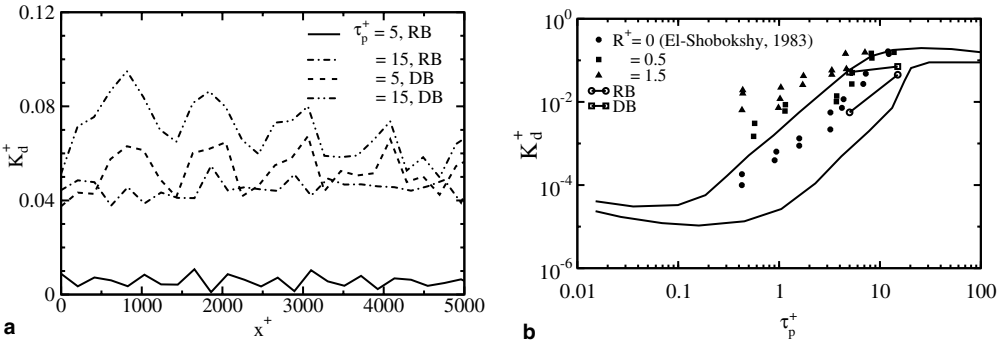

Fig. 7. (a) Deposition coefficients at the interface/wall and (b) comparison to experiments.

Table 1
Deposition coefficients at the interface/wall

Study	Flow	$\tau_p^+ = 5$	$\tau_p^+ = 15$
Liu and Agarwal (1974) (Expt.)	Wall	0.015	0.135
van Haarlem et al. (1998) (DNS)	Wall	0.0064	0.051
Narayanan et al. (2003) (DNS)	Wall	0.0056	0.045
Present work (DNS)	Interface	0.052	0.071

In their experiment on particle laden pipe flows, Liu and Agarwal (1974) found the deposition rate varying quadratically with the particle relaxation time, a result further validated in other experiments and numerical simulations (e.g. McCoy and Hanratty (1975); Young and Leeming (1997)). This relationship is clearly valid for the data presented in Table 1 for particle deposition on a rigid wall (the ratio of the deposition coefficients being approximately equal to the ratio of the square of the response times), but not for the deposition rates in the presence of interfacial waves. In fact, in the DB case, the deposition coefficient for $\tau_p^+ = 5$ is of the same order of magnitude as for $\tau_p^+ = 15$. A clearer understanding of the mechanisms of deposition and their relative importance is necessary to understand this phenomenon.

The deposition rates predicted by the simulations of van Haarlem et al. (1998) and Narayanan et al. (2003) for the RB case were lower than the experimental data (Liu and Agarwal, 1974) and the correlation (McCoy and Hanratty, 1975)

$$K_d^+ = 3.25 \times 10^{-4} \tau_p^{+2}. \tag{9}$$

However, considerable uncertainty and differences exist in the conditions of the various experiments which were mostly conducted for particle deposition in vertical pipes at Reynolds numbers higher than in the DNS studies. Nevertheless, the values obtained fall within the experimental range on which, for example, the above correlation is based. The current model does not take into account effects forces arising due to near-wall interactions, which could have an impact on deposition. The idealization of the flow problem in this study can claim to accurately capture the flux of particles towards the lower boundary for dilute suspensions and their tendency to accumulate there. It can also capture the free-flight mechanism of particle deposition, which is a significant contributor for $\tau_p^+ = 15$ particles, as to be shown in Section 4.6.

4.5. Deposition onto rough walls

Given the interfacial motion, a comparison with particle deposition onto rough walls might be more appropriate because roughness also has the effect of increasing near-wall turbulence intensity. Fig. 7(b) shows the data obtained from the present DNS study along with the rough-wall experimental data of El-Shobokshy (1983) and an envelope including various experimental data on deposition onto smooth walls. The envelope has been extracted from a compilation of experimental data by Young and Leeming (1997) (Fig. 1), that includes results of Liu and Agarwal (1974) and Friedlander and Johnstone (1957), among others. The rough-wall experiments of El-Shobokshy (1983) were performed for roughness sizes of $R^+ = 0.5$ and 1.5, compared to the rms wave amplitude of $f^+_{\mathrm{rms}} = 0.7$. The degree of roughness in the experiment was estimated using the center line average, defined as the average deviation of the surface from a mean or center line. The experimental results show an increase in the deposition rate with roughness, where the increase is more significant for smaller particle inertia. This trend lends further support to the results obtained in this study. Note that, the results obtained in this study would not be applicable to cases with larger roughness elements (roughness over a land surface) where the elements are no longer immersed in the viscous sub-layer. The current results could be extrapolated to higher Reynolds numbers only as long as the roughness in wall units remains comparable.

4.6. Mechanisms of particle deposition

The velocities of depositing particles are analyzed below to identify the dominant mechanisms of particle deposition and explain the observed changes in deposition rates. It is appropriate to mention that throughout the simulation period, no interception of particles by the wave crests was observed. This was due to the wave oscillation being slow enough (see Section 3) for the particles to respond to. Therefore, although the interception of particles could be an additional mechanism of deposition, it never occurred in the flow considered.

4.6.1. Diffusional and free-flight deposition

For the RB case, the depositing particles were divided into two populations (Narayanan et al., 2003): population A with low deposition velocities (roughly equal to the fluid velocity fluctuations in the region close to the wall/interface where particles accumulate; refer to Fig. 5), and population B with high deposition velocities. Population A particles were said to undergo *diffusional deposition* and population B particles were referred to as *free-flight* particles.

Fig. 8 shows the cumulative distribution function (CDF) of the vertical velocities of particles depositing (w_{dep}) at the lower boundary. A large increase in the CDF starting at $-w_{\mathrm{dep}} \approx 0.01$ for the DB case and $-w_{\mathrm{dep}} \approx 0.001$ for the RB case can be observed for both particle response times. These critical numbers are not surprising and represent the turbulent intensity of particles in the vertical direction in the near-wall/interface location, where a peak in their concentration occurs (refer Figs. 5 and 4). In the RB case, almost 90% of $\tau^+_{\mathrm{p}} = 5$ particles deposit via diffusional deposition and the remaining 10% by free-flight. For $\tau^+_{\mathrm{p}} = 15$ particles, the corresponding fractions are 60% and 40%, respectively. In the DB case, about 97% of the $\tau^+_{\mathrm{p}} = 5$ particles deposit via diffusional deposition. The fractions for $\tau^+_{\mathrm{p}} = 15$ remain unchanged. Note that the CDF is a number fraction, and contains no information about the total number of particles depositing.

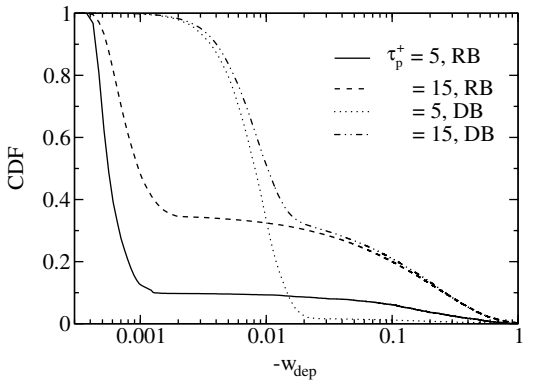

Fig. 8. Cumulative distribution function of the normal velocity of depositing particles.

Due to the increased turbulence intensity near the interface, diffusional deposition for $\tau_p^+ = 5$ particles is greatly enhanced in the DB case. This results in a lower accumulation near the interface and a higher concentration in other regions. Such an increase in the particles located away from the lower boundary could result in higher free-flight deposition, purely because of the availability of more particles. However, since $\tau_p^+ = 5$ particles do not have enough inertia, this secondary effect would not be significant. Thus, for $\tau_p^+ = 5$ particles the importance of diffusional deposition increases further. For $\tau_p^+ = 15$ particles, free-flight is a significant contributor to overall deposition in the RB case. Therefore, although the near-interface turbulence in the DB case results in higher diffusional deposition, the increase in concentration in the bulk as compared to the RB case would also result in a higher incidence of free-flight deposition. No difference in the relative importance of the two mechanisms is seen for $\tau_p^+ = 15$ particles, even if the overall deposition in the DB case is around 60% higher than in the RB case.

4.6.2. Particle residence time analysis

The two deposition mechanisms discussed above were so far distinguished only on the basis of deposition velocity. To make the distinction more evident, the time spent by a particle in a slab three wall units thick adjacent to the interface/wall before depositing, has been recorded. The results are presented in Fig. 9(a) and (b), for $\tau_p^+ = 5$ and $\tau_p^+ = 15$, respectively. The figures show a scatter plot of particle vertical deposition velocity versus particle residence time. The two populations of diffusional and free-flight particles are now better distinguished in combination with their residence times. The free-flight population can be more precisely defined as particles having both a high deposition velocity and a short residence time, and the diffusional deposition particles as those having very small deposition velocities and very large residence times.

As seen from the figures, diffusional deposition particles in the DB case not only have higher deposition velocities, but also smaller residence times. In fact, since the zone near the wavy interface is more active in terms of vertical velocity fluctuations, fluid motions strong enough to make a particle deposit are more frequent in the DB case, so that the residence time is lower. For the free-flight particles, it is evident from the figure that a clear functional relationship exists between the deposition velocity and the residence time. An equation relating the deposition velocity of free-flight particles and their residence times (t_{res}) was developed by Narayanan et al. (2003), given as

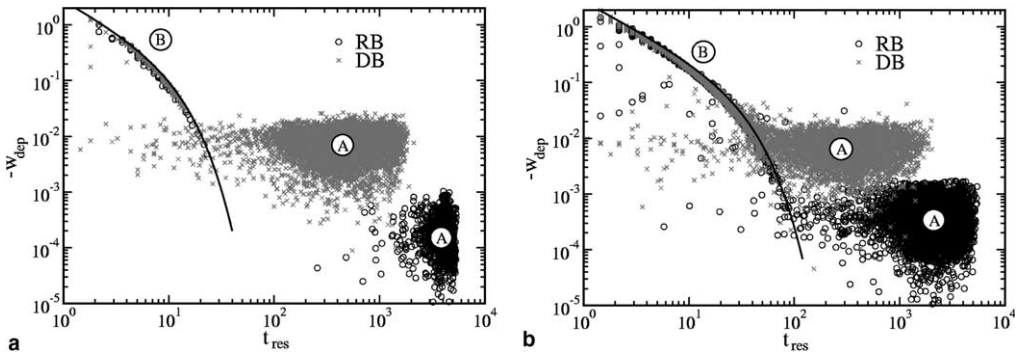

Fig. 9. Scatter plot of the residence time of particles in the slab ($0 \leqslant z^+ \leqslant 3$) versus deposition velocity: (a) $\tau_p^+ = 5$; (b) $\tau_p^+ = 15$; (A) diffusional deposition and (B) free-flight deposition.

$$w_{dep} = \frac{h_s}{\tau_p^+[1 - \exp(\frac{t_{res}}{\tau_p^+})]}, \tag{10}$$

where h_s is the height of the slab chosen for the residence time analysis. This expression matches almost exactly the actual behaviour obtained by the DNS for particles with $\tau_p^+ = 5$ as well as 15, as shown by the continuous line in the figures for both RB and DB cases. The equation was derived by assuming that the free-flight particles have much higher vertical velocities than the fluid fluctuations in the slab. As the velocity of the particles entering the slab becomes smaller and comparable to the fluid fluctuation intensity in the region, it is no longer appropriate to neglect the effect of the fluid velocity fluctuations on the particle path, and the assumption of free-flight does not hold any more. Particles now do not have sufficient momentum to deposit directly and remain in the slab for longer periods of time until they deposit by a random process due to the fluctuations near the interface/wall.

For $\tau_p^+ = 5$, almost all the deposition occurs because of the fluctuations near the wall/interface. Since there is a high concentration of particles near the wall, the increased turbulence in the DB case results in a remarkable increase in the deposition rate for these particles. In contrast, a significant fraction of $\tau_p^+ = 15$ particles deposit via free-flight. Since free-flight does not involve any phenomena occurring near the interface, it can be argued that it is not sensitive to the type of boundary (rigid or deformable). Thus, a less marked increase in deposition for $\tau_p^+ = 15$ is observed, invalidating the often used correlation, in which the deposition rate is made proportional to the square of the particle response time for the range of response times considered here.

5. Summary and conclusions

Lagrangian tracking of particles considering one-way coupling between particles and fluid has been carried out in the gaseous phase of a stratified, counter current, air–water flow calculated using DNS. The interface separating the two continuous phases was free to deform, but restricted to small wave slope deformations ($ak = 0.01$) in the gravity-capillary regime. The results were compared to those obtained by Narayanan et al. (2003) for a wall-bounded open channel flow with the same flow parameters, and to other experimental and numerical data. The influence of gravity on the particle motion was neglected.

The mean and rms velocity profiles for the flow over a wavy interface were almost the same as for the wall-bounded flow, except in the region very close to the interface ($z^+ < 3$). In this region, the fluid turbulence intensity remained finite in the case of the deformable boundary, and resulted in a higher particle phase turbulence intensity in the region.

Much the same way as in wall-bounded turbulence, particles migrate towards the interface and accumulate in the region neighbouring the interface due to turbophoresis. The accumulation was much lower in the deformable boundary case as compared to the wall-bounded case. This was due to the much greater deposition rates caused by the higher turbulence intensity near the deformable interface. A remarkable aspect was the approximately eightfold increase in deposition for $\tau_p^+ = 5$ particles, as compared to the rigid-boundary case. The deposition of $\tau_p^+ = 15$ particles showed an increase of only 60%. For the deformable boundary case, both particle inertias showed almost the same deposition rate, whereas they differed by an order of magnitude for the rigid boundary case. Thus, the well established correlation for wall-bounded flows, where the deposition rate is made proportional to the square of the particle response time is no longer valid in the deformable-boundary case (or flows with enhanced near-wall turbulence). Comparison with experimental data on particle deposition onto rough walls was found to be more appropriate, where a similar increase in the deposition of particles having lower inertia has been observed.

Particle deposition was accounted for by two mechanisms: diffusional deposition and free-flight deposition. The two mechanisms were clearly demarcated by a residence-time analysis where the residence time of a particle before deposition in a thin region adjacent to the interface was calculated. It was shown that most of the small-inertia particles deposited by diffusional deposition, whereas up to 40% of $\tau_p^+ = 15$ particles deposited by free-flight. The free-flight deposition process was not affected by the interfacial motion, as those particles attained their high deposition velocities at locations away from the direct zone of influence of the interface. For $\tau_p^+ = 15$ particles, the relative significance of the two mechanisms remained unaltered and also the increase in the deposition rate was not so dramatic as in the case of $\tau_p^+ = 5$ particles.

Acknowledgements

The authors appreciate the support of Prof. George Yadigaroglu and would like to thank Prof. Sanjoy Banerjee and Dr. Valerio De Angelis (UCSB) for making available the isothermal version of the DNS code employed in this study. L.B. (coming from the University of Udine, Italy) gratefully acknowledges the financial support by the Nuclear Engineering Laboratory during his stay at ETH-Zurich. C.N. acknowledges the funds provided by the European Research Community on Flow Turbulence and Combustion (ERCOFTAC), through the Leonhard Euler Center, Switzerland. Part of the computations were performed on the NEC SX-5 at the Swiss Center for Scientific Computing (CSCS) in Manno, Switzerland.

References

Brooke, J.W., Hanratty, T.J., McLaughlin, J.B., 1994. Free-flight mixing and deposition of aerosol. Phys. Fluids 6, 3404.

Brooke, J.W., Kontomaris, K., Hanratty, T.J., McLaughlin, J.B., 1992. Turbulent deposition and trapping of aerosol at the wall. Phys. Fluids A 4, 825.

Chamberlain, A.C., 1967. Transport of lycopodium spores and other small particles to rough surfaces. Proc. R. Soc. A. 296, 45–70.

Cleaver, J.W., Yates, B., 1975. A sub-layer model for the deposition of particles from a turbulent flow. Chem. Eng. Sci. 30, 983.

Clift, R., Grace, J.R., Weber, M.E., 1978. Bubble, Drops and Particles. Academic Press, New York.

DeAngelis, V., Lombardi, P., Banerjee, S., 1997. Direct numerical simulation of turbulent flow over a wavy wall. Phys. Fluids 9, 2429.

El-Shobokshy, M.S., 1983. Experimental measurements of aerosol deposition to smooth and rough surfaces. Atmos. Environ. 17, 639–644.

El-Shobokshy, M.S., Ismail, I.A., 1980. Deposition of aerosol particles from turbulent flow onto rough pipe wall. Atmos. Environ. 14, 297–304.

Elghobashi, S., Truesdell, G.C., 1992. Direct simulation of particle dispersion in a decaying isotropic turbulence. J. Fluid Mech. 242, 655.

Friedlander, S.K., Johnstone, H.F., 1957. Deposition of suspended particles from turbulent gas streams. Ind. Eng. Chem. 49, 1151.

Fulgosi, M., Lakehal, D., Banerjee, S., DeAngelis, V., 2003. Direct numerical simulation of turbulence in a sheared air–water flow with deformable interface. J. Fluid Mech. 482, 319–345.

Kaftori, D., Hetsroni, G., Banerjee, S., 1995. Particle behaviour in the turbulent boundary layer: motion, deposition and entrainment. Phys. Fluids 7, 1095.

Liu, B.Y.H., Agarwal, J.K., 1974. Experimental observation of aerosol deposition in turbulent flow. J. Aerosol Sci 5, 145.

Marchioli, C., Soldati, A., 2002. Mechanisms for particle transfer and segregation in turbulent boundary layer. J. Fluid Mech. 468, 283.

Maxey, M.R., Riley, J.K., 1983. Equation of motion for a small rigid sphere in a nonuniform flow. Phys. Fluids 26, 883.

McCoy, D.D., Hanratty, T.J., 1975. Rate of deposition of droplets in annular two-phase flow. Int. J. Multiphase Flow 3, 319.

McCready, M.J., Hanratty, T.J., 1985. Effect of air shear on gas absorption by a liquid film. AIChE J. 31, 2066.

McLaughlin, J.B., 1989. Aerosol particle deposition in numerically simulated channel flow. Phys. Fluids 1, 1211.

Mito, Y., Hanratty, T.J., 2003. A stochastic description of wall sources in a turbulent field. Part 1: verification. Int. J. Multiphase Flow 29, 1373–1394.

Miyake, Y., Tsujimoto, K., Nagai, N., 2002. Numerical simulation of channel flow with a rib-roughened wall. J. Turbulence 3.

Narayanan, C., Lakehal, D., Yadigaroglu, G., 2002. Linear stability analysis of particle-laden mixing layers using lagrangian particle tracking. Powder Tech. 125, 122.

Narayanan, C., Lakehal, D., Botto, L., Soldati, A., 2003. Mechanisms of particle deposition in a fully-developed turbulent open channel flow. Phys. Fluids 15, 763.

Rashidi, M., Hetsroni, G., Banerjee, S., 1990. Particle-turbulence interaction in a boundary layer. Int. J. Multiphase Flow 16, 935.

Reeks, M.W., 1983. The transport of discrete particles in inhomogeneous turbulence. J. Aerosol Sci. 14, 729.

van Haarlem, B., Boersma, B.J., Niewstadt, F.M.T., 1998. Direct numerical simulation of particle deposition onto a free-slip and no-slip surface. Phys. Fluids 10, 2608.

Wang, Q., Squires, K.D., Chen, M., McLaughlin, J.B., 1997. On the role of lift force in turbulence simulations of particle deposition. Int. J. Multiphase Flow 23, 749.

Young, J., Leeming, A., 1997. A theory of particle deposition in turbulent pipe flow. J. Fluid Mech. 340, 129.

Zhang, H., Ahmadi, G., 2000. Aerosol particle transport and deposition in vertical and horizontal turbulent duct flows. J. Fluid Mech. 406, 55–80.